Optics Communications 358 (2016) 35–44

Contents lists available at ScienceDirect

Optics Communications

journal homepage: www.elsevier.com/locate/optcom

Designing coherent optical wireless systems for high speed indoor telecom applications

Thomas Kamalakis [a,*], Panagiotis Kanakis [a], Adonis Bogris [b], Vasilis Dalakas [a], Georgia Dede [a]

[a] Department of Informatics and Telematics, Harokopio University, Omirou 9, Athens 17671, Greece
[b] Technological Educational Institute of Athens, Department of Informatics, Aghiou Spiridonos, Egaleo 12243, Greece

ARTICLE INFO

Article history:
Received 26 July 2015
Received in revised form
31 August 2015
Accepted 2 September 2015
Available online 18 September 2015

Keywords:
Optical wireless
Coherent detection
Local area networks

ABSTRACT

This paper focuses on several design issues of coherent optical wireless systems as a means of providing high data rate optical links in indoor environments enabling the realization of ultra-broadband wireless local area networks. We show how the performance specifications can be translated into signal-to-noise ratio requirements inside the coverage area, taking into account the laser phase noise mitigation scheme. We then discuss the power budget details using Gaussian beam optics incorporating the transceiver positioning and the optical systems used at the transmitter and receiver side. We also treat the influence of ambient light noise. We show that coherent optical wireless systems are characterized by excellent signal-to-noise performance enabling networking at very high data rates. Our results indicate that 2 Gb/s and 10 Gb/s data rates can be easily sustained at 3 m distances over a circular coverage area of 1 m radius using Class-1 lasers for the transmitter and the local oscillator. We also discuss the power gain compared to intensity modulated/direct detection optical wireless and show that it can be as high as 20 dB, especially near the edge of the coverage area.

1. Introduction

The distribution of online content through the world-wide web is expected to dominate video entertainment offering in the years to come. Various applications such as high-definition video surveillance, tele-presence and peer-to-peer networking put stringent requirements in the capacity of access and home/office networks. The advent of 4 K video distribution will not be fully supported unless multi-gigabit data rates become available at these domains. Fiber-to-the-home (FTTH) [1,2] is already being considered as a technology of choice for the realization of broadband access networks in many countries around the globe. Passive optical networks (PONs) [3] can support unrivaled access data-rates at the customer premises extending beyond 1 Gb/s, especially if wavelength division multiplexing (WDM) is applied [4,5]. The question now becomes how this broadband traffic can be distributed inside the home/office environment. Optical wireless may hold the key for overcoming this obstacle combining fiber-like data rates and the merits of wireless solutions including flexibility, mobility and cable-free installation in existing dwellings [6,7]. Data center networking [8] is another potential market for such ultra-high speed wireless technologies [9] alleviating the cost associated with fiber cable deployment and management. Optical wireless systems mainly rely on intensity modulation/direct detection (IM/DD) using either the infrared or visible spectrum [10]. Such links are shown to provide high data rates but can be impaired by ambient light noise and the multi-path nature of the optical wireless channel with direct detection.

In this paper, building on the existing know-how of IM/DD optical wireless, we investigate the potential of coherent optical wireless systems (COWS) [11–13] for establishing a multi-gigabit short range optical link and present a detailed system design framework covering various aspects of the system. The primary motivation behind our study is the inherent power gain of a coherent receiver which may lead to reduced transmission power requirements. Our results demonstrate the suitability of COWS for establishing ultra-broadband wireless local area networks intended for data center and local area networking. Compared to previous studies in the area of indoor COWS, the paper contributes in the following points: first, we include the effect of laser phase noise mitigation using digital signal processing and how it impacts the power budget of the link through the required receiver signal-to-noise ratio (SNR). Second, we highlight several aspects of the nature of the coherent optical wireless channel, which unlike conventional IM/DD is practically immune to multipath interference. We show that in integrated or fiber-coupled coherent

* Corresponding author. Fax: +30 210 9549401.
E-mail address: thkam@hua.gr (T. Kamalakis).

http://dx.doi.org/10.1016/j.optcom.2015.09.014
0030-4018/

receivers, ambient light does not couple well with the input waveguide mode or the local oscillator field and provide equations for the ambient light coupling efficiency. Using Gaussian optics, that are arguably more suitable for laser beam propagation than simpler Lambertian radiation patterns, we provide a detailed framework for the power budget analysis using ABCD matrix theory. We pay particular importance to transmitter and receiver optics. We show that a wide enough area can be covered using a two lens system at the transmitter and determine the required receiver optical system parameters. We highlight the relation between the transmitter power receiver area product $P_T A_r$ and the overall system performance and discuss the influence of residual ambient light noise. In addition we compare the performance of coherent and IM/DD optical wireless and show that the former requires much less power to achieve the same error rate and that the corresponding gain may be as high as 20 dB depending on the position inside the coverage area and the data rate. Our results indicate that 2 Gb/s and 10 Gb/s data rates can be easily sustained at 3 m distance over a circular coverage area of 1 m radius using Class-1 eye safe lasers for the transmitter and the local oscillator. Such a system therefore fulfills many of the requirements posed by next generation local area networks. The results of the paper indicate that although IM/DD optical wireless is cost-effective, coherent optical wireless requires much less power, no equalization scheme to mitigate the frequency dependence of the channel while at the same time provide the well-known spectral efficiency of coherent detection enabling dense wavelength division multiplexing in order to meet data rate requirements imposed in large server farms [14].

The rest of the paper is organized as follows: in Section 2, we present the architecture of a coherent optical wireless link, highlighting various components that play an important role in the design procedure including the modulator, transmitter optics, free space propagation, receiver optics and the achieved SNR at the coherent receiver. In Section 3, we examine the receiver SNR requirements imposed by phase modulation schemes such as

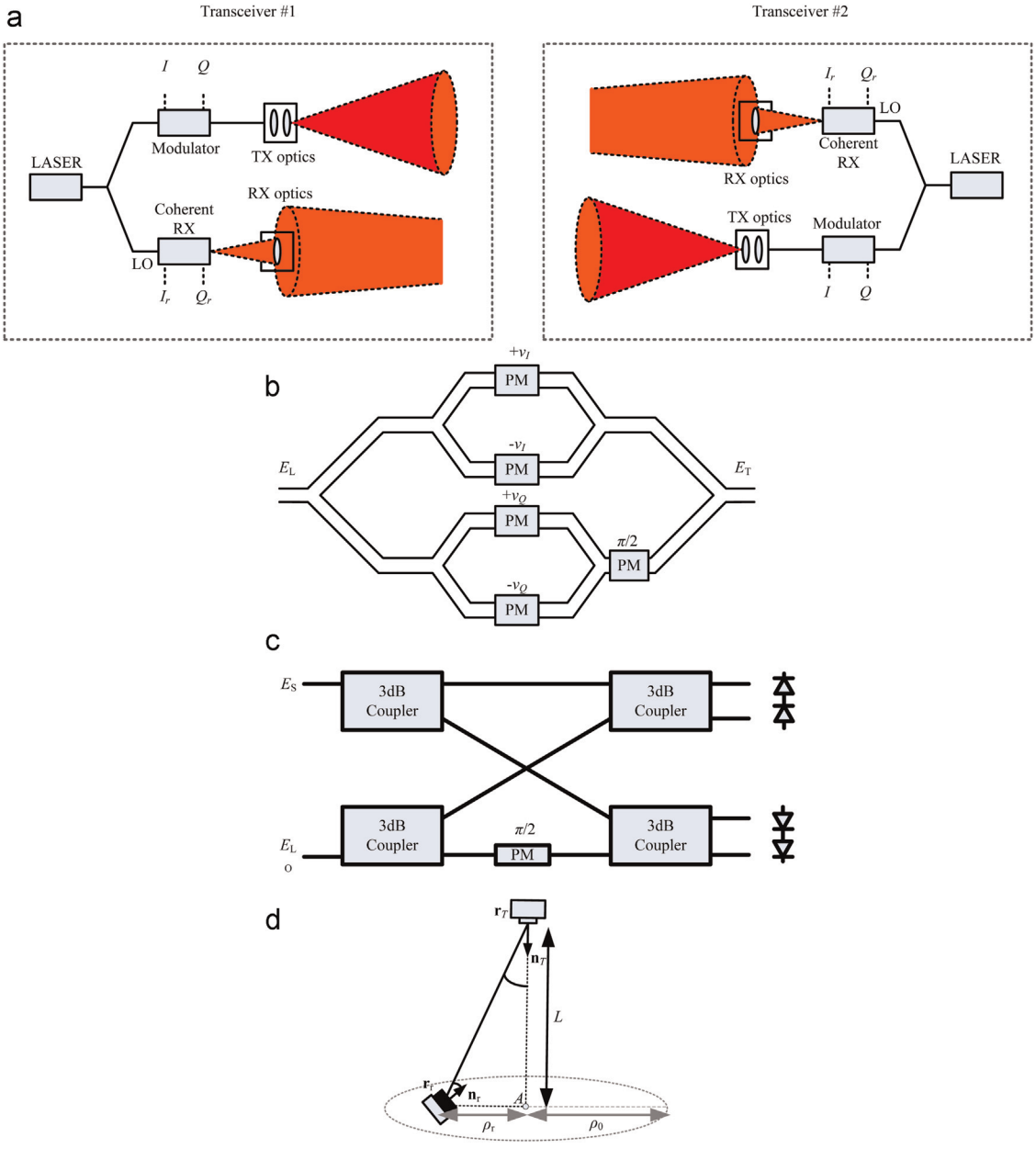

Fig. 1. System under consideration: (a) coherent transceivers possibly employing a single laser at each side, (b) an I/Q modulator, (c) a coherent receiver based on a 90° optical hybrid and (d) transceiver placement.

quadrature phase shift keying (QPSK) and the impact of laser linewidth. Based on the two previous sections, we carry out a detailed system design in Section 4, where we investigate the performance of the COWS systems in terms of achieved SNR and coverage. We highlight the tradeoff between transmitter power and receiver area and discuss the impact of ambient light noise in more detail. In Section 5, we compare the coherent and IM/DD systems and calculate the power gain obtained by the former. Some concluding remarks are given in Section 6.

2. System under consideration

The COWS transceiver under investigation is presented in Fig. 1 (a). In order to limit the number of required optical components, we may choose to use a single laser source at each link side. As shown in Fig. 1(a), this laser can be used as a source for transmitting the downlink data and as a local oscillator for the uplink signal. In this manner, the light beam of the laser source is divided by a 3 dB splitter into two branches. At the left transceiver, the upper branch is fed to an I/Q modulator [15], that imprints the signal to be transmitted in the optical field. The structure of the modulator is shown in Fig. 1(b). In the case of PSK modulation, a simpler phase modulator can also be used instead. The field exiting the modulator passes through the transmitter optics consisting of a number of diverging lenses that are used for widening the beam and achieving the required coverage at the receiver plane at the opposing side. In this paper, we assume that the optical systems of both the transmitter and the receiver comprise of simple lenses. The use of a diffuser has been suggested in the past [11,12] in order to provide a more uniform illumination but may degrade the coherence properties of the wave and therefore limit the coupling efficiency at the receiver, as we shall discuss in Section 4.4.

The lower branch acts as the local oscillator of the coherent receiver for the uplink data. The coherent receiver can be heterodyne or homodyne, with the latter providing a 3 dB SNR gain compared to the former [16]. The optical field at the receiver side is collected by the receiving lens and is focused on the input port of the coherent receiver. Various implementation strategies can be adopted for the coherent receiver. In this paper, we assume an optical hybrid-based phase-diversity homodyne receiver [17] widely used in fiber-optic systems that is depicted in Fig. 1(c). Fig. 1(d) shows the arrangement of a transmitter/receiver pair in a typical indoor scenario. The coverage area is determined by the beamwidth at the receiver plane which should be chosen wide enough to ensure link flexibility and mobility. Depending on the application scenario one must seek a compromise between transmitter and local oscillator power, receiver area and system coverage.

2.1. Transmitter model

The optical field E_0 exiting the modulator output can be modeled as a modulated Gaussian beam propagating along the z-axis [18], i.e.

$$E_0 = \frac{u_0(\boldsymbol{\rho})}{2}(I + jQ), \tag{1}$$

where $\boldsymbol{\rho}=(x,y)$, while I and Q are the amplitudes for the in-phase and the out-of-phase signals respectively and are related to the corresponding driving voltages, $I=\cos(\pi v_I/V_\pi/2)$ and $Q=\cos(\pi v_Q/V_\pi/2)$ [18], V_π is the half-wave switching voltage of the modulator, while $u_0(\boldsymbol{\rho})$ is the unmodulated Gaussian beam profile [19], §16.3,

$$u_0(\boldsymbol{\rho}) = \sqrt{\frac{2P_T}{\pi w_0^2}}\exp\left(-\frac{jq_0k}{2}\rho^2\right). \tag{2}$$

In (2), P_T is the power of laser beam at the modulator input, w_0 is the initial beamwidth of the laser beam, $\rho=|\boldsymbol{\rho}|$, $k=2\pi/\lambda$ is the propagation constant in free space while the parameter $q=q(w,R)$ is determined by the wavelength λ, the width w and the curvature R of the beam,

$$\frac{1}{q(w,R)} = -j\frac{\lambda}{\pi w^2} + \frac{1}{R} \tag{3}$$

The parameter $q_0=q(w_0,R_0)$ in (2) is obtained from (3) by replacing $w=w_0$ and $R=R_0$ where R_0 is the initial beam curvature which is assumed infinite ($R_0=+\infty$) [19], §17.1, implying that $\mathrm{Re}\{q_0\}=0$. The field in (1) represents the slowly varying field component and the actual field e_T is given by $e_T=E_T\exp(jkz)$. We have also assumed that the field is linearly polarized along a specified direction and hence we need to treat only a single field component. Finally in (2), we have neglected the z-dependent phase variation $\psi(z)$ which plays no role in the subsequent power budget calculations.

The beam can be shaped by the transmitter optics in order to determine the system coverage as we will discuss in Section 4. The transmitter optics consist of a number of lenses N of focal length f_μ which are spaced d_μ apart. The properties of the beam at the receiving plane can be determined through the 2×2 ABCD matrix $\mathbf{M}_{\mathrm{tot}}$ of the system [20] which is written as the following product:

$$\mathbf{M}_{\mathrm{tot}} = \begin{bmatrix} A & B \\ C & D \end{bmatrix} = \mathbf{L}(d_0)\mathbf{M}(f_1)\mathbf{L}(d_1)\cdot\ldots\cdot\mathbf{M}(f_N)\mathbf{L}(d_N). \tag{4}$$

In (4), the matrices $\mathbf{L}$ and $\mathbf{M}$ describe the ABCD matrices of the free space propagation between the lenses and the lenses respectively and are given by:

$$\mathbf{L}(d) = \begin{bmatrix} 1 & d \\ 0 & 1 \end{bmatrix}, \tag{5}$$

$$\mathbf{M}(f) = \begin{bmatrix} 1 & 0 \\ -1/f & 1 \end{bmatrix}. \tag{6}$$

In (4), d_0 is the distance between the source and the first lens ($\mu=1$), while d_μ for $1\le\mu\le N-1$ is the distance between the μth and $(\mu+1)$th lenses and $d_N=L$ is the propagation distance between the transmitter and the receiver plane shown in Fig. 1(d). Given the elements of the ABCD matrix, the parameter $q=q_r$ of the beam at the receiver plane is determined by the following equation [20],

$$q_r = q(w_r, R_r) = \frac{Aq_0 + B}{Cq_0 + D} \tag{7}$$

The beamwidth w_r and the beam curvature R_r can be calculated from (7) and (3). We can also estimate the value of the q parameter, $q=q_T$, at the output of the optical transmitter system using the ABCD matrix in (4) omitting the last stage corresponding to free space propagation, i.e. applying the matrix $\mathbf{M}_{\mathrm{T}}=\mathbf{M}_{\mathrm{tot}}\mathbf{L}^{-1}(L)$. We can then relate q_r with q_T by using (7) and replacing the elements of the ABCD matrix $\mathbf{M}_{\mathrm{tot}}$ with those of free space $\mathbf{L}(L)$ in (5) i.e. setting $A=1$, $B=\mathrm{d}$, $C=0$ and $D=1$ which readily yields $q_r=q_T+L$. According to (3), this implies that $1/R$ is increased by L. Since the free space propagation L is much larger than the propagation distances between the lenses, the curvature of the wave at the receiver is essentially determined by $R_r\cong 1/L$. This implies that the incident wave E_r at the receiving plane acquires a parabolic phase variation $\sim\exp(-j\rho^2/2/L)$.

2.2. Receiver optics

The analysis of the receiver optics is somewhat more involved, since the receiving lens focuses only a part of the incoming beam and therefore the ABCD formulation cannot be used. The received field is written as:

$$E_r = \frac{u_r(\boldsymbol{\rho})}{2}(I + jQ), \tag{8}$$

where $u_r(\boldsymbol{\rho})$ is obtained from (2) by replacing w and q with w_r and q_r respectively. If the beamwidth w_r is much larger than the receiving lens dimensions, then we can assume that the incident beam has nearly constant amplitude $|u_r(\boldsymbol{\rho})| \cong u_{r0}$ over the receiving lens. To better understand light focusing on the receiving lens, we assume that the receiver is placed below the transmitter (point A in Fig. 1(d)) and that their orientations are aligned, i.e. $\mathbf{n}_T = -\mathbf{n}_r$. In this case, the field incident on the receiving lens is described as $u_i(\boldsymbol{\rho}) = u_r(\boldsymbol{\rho})$ for $\rho \le a$ where a is the radius of the receiving lens and $u_i(\boldsymbol{\rho}) = 0$ for $\rho > a$ where $\rho = |\boldsymbol{\rho}|$. Taking into account the $\exp(-j\rho^2/2/L)$ phase variation of the incident beam we can therefore write,

$$u_i(\boldsymbol{\rho}) \cong \begin{cases} u_{r0}\exp(-j\rho^2/2/L), & \rho \le a \\ 0, & \rho > a \end{cases}. \tag{9}$$

The receiving lens adds an additional phase component $\exp(jk\rho^2/2/f_r)$ and the image $u_F(\boldsymbol{\rho})$ formed at distance s is determined by the 2D Fourier transform [21], §5.2,

$$u_F(x, y) = \frac{j}{\lambda d}\int_{-\infty}^{+\infty} dx_1 \int_{-\infty}^{+\infty} dy_1 u_R(\rho_1) e^{j\frac{k\rho_1^2}{2f_r}} e^{-\frac{jk}{2s}|\boldsymbol{\rho}-\boldsymbol{\rho}_1|^2}, \tag{10}$$

where $\boldsymbol{\rho}_1 = (x_1, y_1)$. The integral above can be readily evaluated in the case where $s^{-1} = f_r^{-1} - L^{-1}$ in which case the parabolic phase terms cancel out. Using a change of variables in the polar coordinate system, $x_1 = \rho_1 \cos\varphi_1$ and $y_1 = \rho_1 \sin\varphi_1$ and applying the properties of Bessel functions [22], §9.1.21, we readily obtain:

$$u_F(\rho) = \frac{j2\pi u_{r0} a^2}{\lambda s}\frac{J_1(u)}{u}\exp\left(-j\frac{\pi\rho^2}{\lambda s}\right), \tag{11}$$

where

$$u = \frac{2\pi a\rho}{\lambda s}. \tag{12}$$

The ratio $J_1(u)/u$ is typical of the Airy pattern distribution formed by a circular lens due to diffraction [21], §4.4.2. It essentially determines the spot size of the image. The field can be assumed confined inside a disk with diameter $D_a \cong 2.44\lambda s/(2a)$. For large enough L we obtain, $s^{-1} = f_r^{-1} - L^{-1} \cong f_r^{-1}$ which implies that $D_a \cong 2.44\lambda(f_r/2a) = 2.44F\lambda$ where $F = f_r/(2a)$ is the F-number of the lens. We therefore deduce that the F-number of the receiving lens determines the spot-size of the focused beam. If the light is to be focused at the input of a single-mode fiber, then D_a should be smaller than $2w_{\text{mode}}$ where w_{mode} is the width of the mode in order to minimize coupling loss. This readily yields an expression for the maximum lens F-number,

$$F \le \frac{w_{\text{mode}}}{1.22\lambda} \tag{13}$$

For example assuming a single mode fiber $a_f = 4$ μm radius and V-number equal to $V = 2.1$, applying Marcuse's formula [23] we find $w_{\text{mode}} \cong a_f\,(0.65 + 1.619\,V^{-3/2} + 2.879\,V^{-6}) \cong 5$ μm and at $\lambda = 1.55$ μm we obtain $F \le 2.62$.

2.3. Power budget and symbol estimates

The power P_r collected by the receiving lens in the case of unmodulated light (i.e. in the absence of the modulator), is given by the integral of the field intensity $|u_i|^2$ on the receiving lens taking into account the lens inclination. Assuming that the receiving lens diameter is much smaller than the beamwidth at the receiving plane, the incident field intensity $|u_i|^2$ can be assumed constant and hence:

$$P_r \cong |u_{r0}|^2 A_r \cos\theta_r = \frac{2P_T A_r \cos\theta_r}{\pi w_r^2} e^{-2\rho_r^2/w_r^2} \tag{14}$$

where A_r is the receiving lens area. The angle θ_r is determined by:

$$\cos\theta_r = \frac{\mathbf{n}_r \cdot (\mathbf{r}_T - \mathbf{r}_r)}{|\mathbf{r}_T - \mathbf{r}_r|} \tag{15}$$

The term $\cos\theta_r$ in (14) account for the inclination of the receiving aperture and typically appears in power budget equations [17]. The field of the received signal E_S and the local oscillator E_{LO} can be written as:

$$E_S = \tfrac{1}{2}\sqrt{P_r}(I + jQ), \tag{16}$$

$$E_{\text{LO}} = \sqrt{P_{\text{LO}}}\, e^{j\phi}, \tag{17}$$

where the ½ factor in (16) follows from the same factor in (1) and P_{LO} is the local oscillator power and ϕ is the phase difference between the unmodulated received signal and the local oscillator field which is determined by the phase noise of the laser sources. The phase difference $\phi(t)$ slowly varies between consecutive symbols and can be modeled as a random walk process [24]. The variation of ϕ between the pth and the $(p-1)$th symbols is given by:

$$\phi(pT_s) - \phi((p-1)T_s) = \Delta\phi_p, \tag{18}$$

where $\Delta\phi_p$ are independent, zero mean Gaussian random variables with variance equal to $<\Delta\Delta\phi_p^2> = 2\pi(\Delta\nu_T + \Delta\nu_r)T_s$ where T_s is the symbol duration, $\Delta\nu_T$ and $\Delta\nu_r$ are the linewidths of the laser at the transmitter and the receiver respectively.

The receiving symbol estimates can be derived by considering the structure of the 90° optical hybrid in Fig. 1(c) [17, 25]:

$$I_r = \frac{R\sqrt{P_{\text{LO}}P_r}}{2}(I\cos\phi - Q\sin\phi) + n_I, \tag{19}$$

$$Q_r = \frac{R\sqrt{P_{\text{LO}}P_r}}{2}(I\sin\phi + Q\cos\phi) + n_Q, \tag{20}$$

where R is the detector responsivity, n_I and n_Q are the additive noise components at the receiver. Note that (19) and (20) are derived by assuming that the polarization state are the same for the local oscillator and the signal. Several techniques can be used to relax this requirement, such as polarization tracking [26], scrambling [27] and diversity [28]. The power spectral density (PSD) of the noise components is given by:

$$S_n \cong qR(P_{amb} + P_{LO}) + \tfrac{1}{2}S_{th}, \tag{21}$$

where we have assumed that the received power P_r is much smaller than the local oscillator power, i.e. $P_r \ll P_{\text{LO}}$ (this will be justified in the power budget calculations in Section 4) and can therefore be ignored in the shot noise calculations. In (21), q is the electron charge, P_{amb} is the power of the ambient light noise coupled at the input of the receiver while S_{th} is the PSD of the

thermal noise. The electrical signal-to-noise ratio in the absence of the laser phase noise is defined as the ratio of the average signal power $<I_r^2>+<Q_r^2>$ to the total noise power $\sigma_I^2+\sigma_Q^2$. The total noise power contains the contribution of the shot and thermal noise and is given by integrating the PSD in (21) inside the receiver bandwidth B. We therefore obtain:

$$\gamma_c^2 = \frac{\langle I_r^2\rangle + \langle Q_r^2\rangle}{\sigma_I^2+\sigma_Q^2} = \frac{\frac{1}{4}R^2P_{\mathrm{LO}}P_r}{2qR(P_{\mathrm{LO}}+P_{\mathrm{amb}})B + S_{\mathrm{th}}B}. \tag{22}$$

In (22), B is the electrical receiver bandwidth which depends on the modulation scheme as we shall discuss in Section 3.

3. Performance requirements

The signal-to-noise ratio calculated in (22) can be related to the performance of the system in terms of the bit-error-rate (BER). Fig. 2 shows the required minimum value of SNR in order to obtain a BER equal to 10^{-3} for QPSK modulation as a function of the linewidth-symbol duration product $\Delta\nu T_s$. We have assumed that the transmitter and the receiver lasers have the same linewidth, $\Delta\nu=\Delta\nu_T=\Delta\nu_r$. We numerically calculated the required SNR based on the symbol estimate equations (19,20). A large number ($\sim 10^7$) of input QPSK symbols $I(p)+jQ(p)=\exp(j\psi_p)$ were generated for various values of SNR and $\Delta\nu T_s$ and the output symbol estimates were calculated by (19) and (20). The samples of the phase noise and amplitude noises were numerically generated based on their statistics, discussed in Section 2.3. We have also implemented the phase recovery scheme described in [29] which relies on differentially precoding the transmitted symbols and carrier phase estimation using digital signal processing at the receiver. In essence, the phase difference $\phi(t)$ is estimated at the receiver by first raising the received symbol estimates $I_r(p)+jQ_r(p)$ to the fourth power which, in the absence of additive noise, removes the modulation-induced phase changes ψ_p. Assuming that the phase difference $\phi(t)$ slowly changes from symbol-to-symbol, its estimate is obtained by averaging the received symbol estimates raised to the fourth power over n_b consecutive bits. In order to retain the correct phase trajectory, the phase estimates must be unwrapped as described in [29]. Given the BER obtained for different values of SNR and $\Delta\nu T_s$ we used 2D interpolation to obtain the SNR values for which the BER is equal to 10^{-3}.

Fig. 2 can be used to appreciate the power penalty induced by the laser phase noise. In the absence of any phase noise ($\phi=0$), the BER P_e for QPSK can be calculated in closed form [30] which yields $P_e=10^{-3}$ for SNR $\cong$9.8 dB. We therefore deduce that depending on the value of the product $\Delta\nu T_s$ and the number of consecutive symbols used in the phase recovery algorithm, the penalty can be up to 6 dB as shown in Fig. 2. We also see that, although a large n_b guarantees small penalties at small linewidth-symbol duration products it can lead to larger penalties as the laser linewidth $\Delta\nu$ is increased, since the phase can no longer be considered constant and the error in the phase estimations increases considerably with the number of consecutive symbols. The figure shows that for $\Delta\nu T_s \le 5\times 10^{-3}$, the minimum required SNR is $\le$16 dB provided the value of n_b is chosen optimally. For a QPSK signal with R_b=2 Gb/s data rate, one obtains $T_s=2/R_b=1$ ns and hence the laser linewidth $\Delta\nu$ must be smaller than 5 MHz. For a 10 Gb/s signal, this limit is relaxed to 25 MHz. Since the laser linewidth of most semiconductor distributed feedback lasers (DFB) ranges from 100 kHz to 10 MHz [17], §2.1, we readily deduce that such lasers can be used especially at high data rates. Employing narrower linewidth lasers can further decrease the power penalty induced by the phase noise.

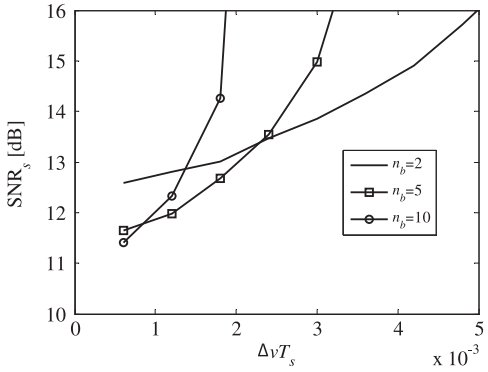

Fig. 2. Required SNR-per-symbol to achieve a bit error rate of $P_b=10^{-3}$ as a function of the linewidth-symbol duration product $\Delta\nu T_s$ for QPSK modulation assuming different number n_b of symbols used in the phase estimation.

4. Design and performance evaluation

Based on the system model outlined in Section 2 and the performance requirements examined in Section 3, we now carry out the COWS design. We initially ignore the ambient light noise which we will later incorporate in more detail. We also neglect multipath-induced distortion. It should be noticed that the nature multipath components in the optical wireless scenario is different than that in conventional radio systems. In the former case, the much larger wavelength leads to significant amount of specular signal reflections. At infrared frequencies, reflections are mostly diffuse, because the surface roughness is comparable or larger than the wavelength, implying that multipath components are only partly coherent. The IM/DD receiver cannot discriminate between coherent and incoherent light, which implies that diffuse components are captured and render the wireless channel frequency-selective [31].

At the coherent receiver, the diffuse multipath signal components will not mix with the line-of-sight component. In the case of a receiver with a bulk 90° hybrid (i.e. with discrete optical components such as splitters, etc.) the diffuse components could propagate inside the hybrid, but they will not match the local oscillator field. These multipath components will also have very small bearing in the noise variance in (21) which is dominated by the shot noise of the local oscillator and the ambient light noise. Alternatively, if the hybrid is realized using single-mode fiber components or in integrated form, then the diffuse field will not couple well with the fundamental waveguide mode at the receiver input in Fig. 1(c) as we shall show in Section 4D. We therefore ignore any diffuse light components in our calculations.

4.1. Data rate and coverage area

When evaluating a wireless technology for indoor applications, the achievable data rate and the coverage area are among the most important parameters [31]. In the case at hand, the performance requirements are met by ensuring a sufficiently high signal-to-noise ratio SNR within the specified coverage area ($\rho_r \le \rho_0$) at the receiver plane as shown in Fig. 1(d). The optimum SNR, is obtained from (22) in the absence of ambient light noise ($P_{\mathrm{amb}}\cong 0$) and assuming that the shot noise is much larger than the thermal noise ($S_{\mathrm{th}}\cong 0$):

$$\mathrm{SNR} = \frac{RP_r}{8qB}, \tag{23}$$

while the maximum SNR is obtained when the receiver is place directly below the transmitter, i.e. at point A in Fig. 1(d):

$$\mathrm{SNR}_{\max} = \frac{RP_{r,\max}}{8qB} = \frac{2P_T}{\pi w_r^2}\frac{RA_r}{8qB}, \tag{24}$$

where $P_{r,\max}$ is the maximum power at point A directly below the transmitter setting $\rho_r=0$ and $\cos\theta_r=1$ in (14). As we move the receiver away from this position, the received power and hence the SNR will decrease. The coverage can be specified in terms of the SNR degradation: at distance $\rho_r=\rho_0$ we specify that the SNR will not be smaller than $K\times \mathrm{SNR}_{\max}$ where K is the maximum SNR degradation factor at the boundaries of the coverage area. Using (14) and assuming that the receiver is oriented towards the transmitter ($\theta_r=0$), Eqs. (23) and (24) readily yield,

$$\frac{P_r(\rho_0)}{P_{R,\max}} = \exp\left(-\frac{2\rho_0^2}{w_r^2}\right) = K. \tag{25}$$

In the presence of alignment errors, the $\cos\theta_r$ in (14) may introduce additional power losses. However even for $\theta_r=\pm\pi/8$, these additional power losses are $l_{\mathrm{extra}}=10\log_{10}(\cos\theta_r)<0.4$ dB. Eq. (25) essentially determines the required beamwidth w_r at the receiver plane,

$$w_r = \rho_0\sqrt{2}(-\ln K)^{-1/2}. \tag{26}$$

Using (24), we can translate this value to a required value for P_TA_r i.e. the transmitter power-receiving area product,

$$P_TA_r = \frac{4q\pi B\rho_0^2\mathrm{SNR}_{\max}}{R}(-\ln K)^{-1}. \tag{27}$$

4.2. System design for 2 Gb/s data rate

In our design, we assume that the wavelength of operation is $\lambda=1550$ nm, widely used in fiber optical systems. There are three reasons behind a wavelength choice in the wireless domain as well. First of all, the majority of the required components (narrow linewidth lasers, I/Q modulators, integrated coherent receivers, etc.) are already commercially available in integrated form at $\lambda=1550$ nm, which may significantly simplify the implementation of the system. At the time of this writing, such components were not readily available at other wavelengths, say at $\lambda\cong800$ nm which is popular band for IM/DD optical wireless systems. The second reason is that at the infrared spectrum, ambient light noise from sunlight [32] or artificial lighting [33] generally decreases with increasing wavelength, implying that larger wavelengths are generally more favorable in terms of the SNR. The third reason for choosing the 1550 nm band is that eye-safety restrictions on laser power are much less stringent at this portion of the spectrum [35].

Table 1 summarizes the design parameters of a 2 Gb/s and a 10 Gb/s system with a coverage area of radius $\rho_0=1$ m. For the 2 Gb/s system, we assume a 1 mW transmission and local oscillator power for the 2 Gb/s which is much lower than the 10 mW limit for Class-1 eye safe transmitters [35]. Table 1 also quotes other design parameters and the justification for their values.

The maximum SNR is specified at 30 dB, while the SNR degradation factor K is taken 10 dB so that the SNR inside the coverage area ($\rho_r\le\rho_0$) will be ≥20 dB which ensures a BER much smaller than 10^{-3} according to Fig. 2. This implies that the COWS hotspot can be used to connect receiver terminals within a circular cell with a diameter of 2 m. In Section 3, we saw that for $\Delta\nu T_s\le5\times10^{-3}$ the required SNR is 16 dB, and we therefore provide an additional 4 dB margin in the power budget in order to cover for modulator excess losses, misalignment losses, etc. Using (26), we readily determine that the beamwidth at the receiver plane is $w_r\cong0.93$ m. According to Table 1, the distance between the transmitter situated at the ceiling and the receiver placed 0.8 m above the floor is taken $L=3$ m which is a typical value for an average height room. To design the transmitter optics we can use the ABCD matrix formulation discussed in Section 2.A. We assume a two lens system ($N=2$) and that the distance between the lenses is equal to the distance between the first lens and the source ($d_0=d_1=d_T$). The lenses are assumed diverging, having a focal length $f=-1$ cm. Using (4)–(7), we estimate the value of w_r in Fig. 3 for various values of d_T. As shown in the figure, the value $w_r=0.93$ m is obtained at $d_T\cong6$ mm which readily determines the distance between the lenses of the transmitter optics.

The transmitter power-receiving area product is given by (27). Assuming $R=1$ A/W in we obtain $P_TA_r/B\cong17.4\ \mathrm{mW}\times\mathrm{cm}^2\times\mathrm{GHz}^{-1}$. For QPSK, the required electrical bandwidth is approximately $B\cong R_b/2$ [30], §7.6.10 which for the 2 Gb/s system translates to $B=1$ GHz and hence, $P_TA_r\cong17.4\ \mathrm{mW}\times\mathrm{cm}^2$. If we therefore choose

Table 1
System parameters.

Parameter	Value	Comments
TX power (P_T)	1 mW ($R_b=2$ Gb/s) 5 mW ($R_b=10$ Gb/s)	$P_T<10$ mW, Class-1 in terms of eye safety at $\lambda=1550$ nm [35]
Wavelength (λ)	1550 nm	Discussed in Section 4.2
TX linewidth ($\Delta\nu_T$)	≤5 MHz ($R_b=2$ Gb/s) ≤25 MHz ($R_b=10$ Gb/s)	Derived from Fig. 2
Initial beamwidth (w_0)	5 μm	Corresponds to a 4 μm single mode fiber with $V=2.2$ (Section 2.2)
Focal distance of TX lenses (f_T)	−1 cm	Chosen in order to minimize the size of the transmitter optics
Transmitted beamwidth (w_T)	1.5 mm	Calculated using ABCD matrix theory in Section 2.1 using the matrix $\mathbf{M}_T$
Number of TX lenses (N)	2	We use two divergent lenses in order to widen the coverage area
TX lens distance (d_T)	6 mm	Calculated in Section 4.2 in order to obtain the desired coverage area
TX position ($\mathbf{r}_T$)	[0, 0, 3.8 m]	Transmitter is placed on the middle of the ceiling
Local oscillator power (P_{LO})	1 mW ($R_b=2$ Gb/s) 5 mW ($R_b=10$ Gb/s)	$P_{\mathrm{LO}}<10$ mW, Class-1 in terms of eye safety at $\lambda=1550$ nm [35]
RX area (A_r)	17.4 cm^2	Derived from (27)
Specified max SNR ($\mathrm{SNR}_{\max}$)	30 dB	Specified high enough to ensure excellent coverage conditions (Section 4.2)
Coverage radius (ρ_0)	1 m	Should suffice in most application scenarios in order to enable mobility
Beamwidth at RX plane (w_R)	0.93 m	Derived from (26)
Specified min SNR at $\rho=\rho_0$ ($\mathrm{SNR}_{\min}$)	20 dB	Specified from Fig.2 allowing some extra margin
RX position ($\mathbf{r}_R$)	[x, y, 0.8 m]	Receiver placed at the height of a typical office furniture
Responsivity (R)	1 A/W	Typical responsivity of commercially available receivers at $\lambda=1550$ nm
Optical filter bandwidth ($\Delta\lambda$)	50 nm	Large enough to ensure order sufficient receiver field-of-view [33]
RX lens diameter ($2a$)	4.7 cm	Assuming circular aperture, $a=(A_r/\pi)^{1/2}$
RX lens focal length (f_R)	≤11.2 cm	Section 4.2
RX linewidth ($\Delta\nu_R$)	Same as TX linewidth	Derived from Fig. 2

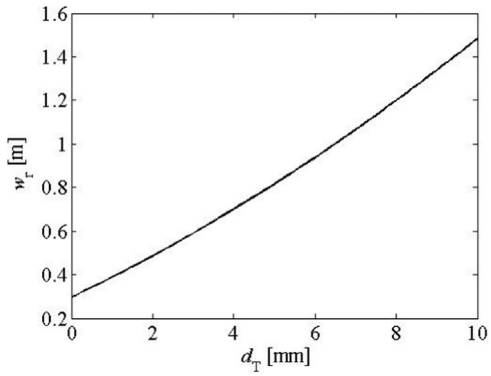

Fig. 3. Variation of the beamwidth at the receiver plane as a function of the transmitter inter-lens distance d_T.

$P_T=1$ mW, we obtain a relatively small area $A_r=17.4$ cm^2 which translates to a circular aperture of diameter $2a=4.7$ cm. We shall see that this small aperture area leads to reduced capturing of the ambient light noise, limiting the associated power penalty. The required focal distance f_r of the receiving lens is determined from the required F-number of the lens $F=f_r/(2a)\leq 2.6$, which turns out to be $f_r\leq 12.3$ cm.

Fig. 4 shows the received power at the receiver plane (x, y, 0.8 m) for the transmitter/receiver arrangement specified in Table 1, assuming that $-1\text{ m}\leq x,y\leq 1$ m. The maximum received power is obtained as expected at $x=y=0$, i.e. directly below the transmitter and is equal to -28.9 dB m. Fig. 5 shows the corresponding SNR obtained at the receiver plane. As expected the achieved SNR is high, peaking at 30 dB as specified in Table 1. In Fig. 6(a) and (b), we show the received power and the SNR along the line $y=0$. It is deduced that the SNR is always ≥ 20 dB inside the coverage area, $\rho\leq\rho_0=1$ m. The maximum SNR degradation is 10 dB and occurs at $\rho_0=1$ m, i.e. at the boundary of the coverage area. We therefore conclude that the system can operate with an acceptable BER, especially given the 4 dB margin adopted with respect to the minimum required SNR≅16 dB calculated in Section 3.

4.3. System design for 10 Gb/s data rate

At higher data rates R_b, one must take into account the corresponding increased electrical bandwidth B. However, the value of the required $P_T A_r/B$ is the same, since B does not otherwise appear in the power budget calculations. For $R_b=10$ Gb/s we obtain $B=5$ GHz and hence this leads to an increased transmitted power-receiver area product $P_T A_r\cong 87$ mW × cm^2. In order to keep the receiver dimensions small, we choose a higher transmitter power $P_T=5$ mW for this system. Fig. 7 shows the obtained receiver

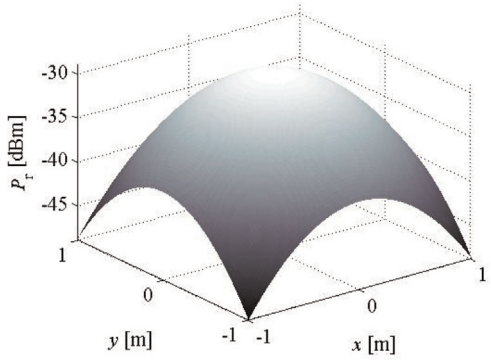

Fig. 4. Surface plot of the estimated received power P_r for the 2 Gb/s system.

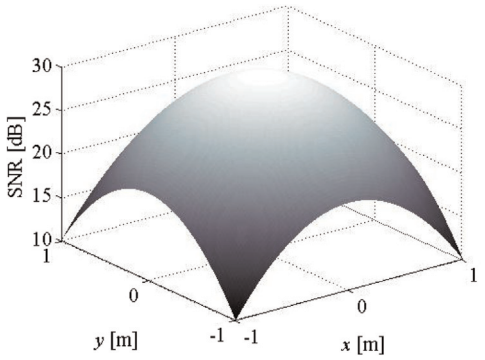

Fig. 5. Surface plot of the estimated signal-to-noise per-symbol ratio for the 2 Gb/s system.

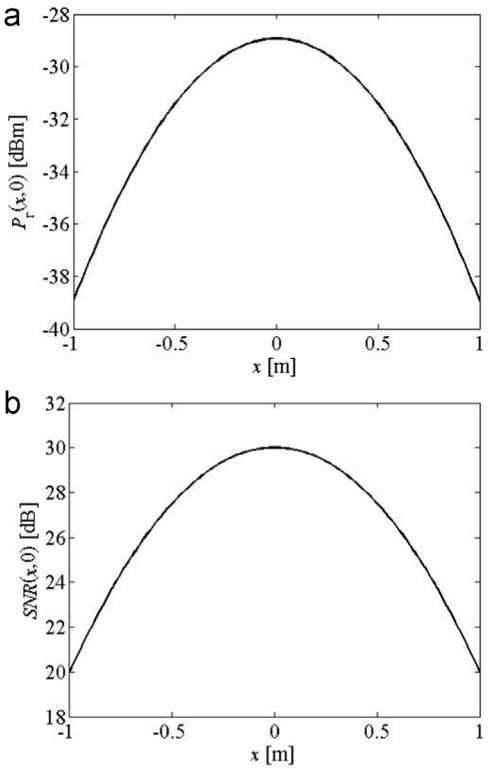

Fig. 6. Estimated (a) received power and (b) achieved SNR per-symbol along the x-axis for the 2 Gb/s system.

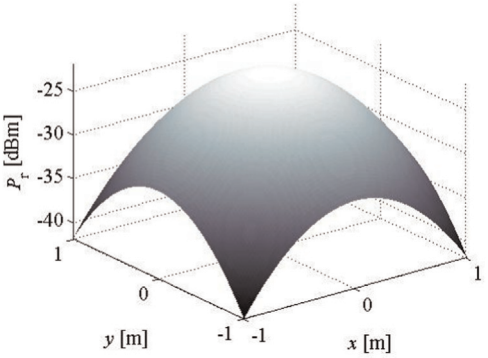

Fig. 7. Surface plot of the estimated received power P_r for the 10 Gb/s system.

power at the receiver plane for this design. Fig. 8 shows the receiver power along the line $x=0$. The obtained SNR is the same as that of the 2 Gb/s shown in Figs. 5 and 6(b). The results indicate

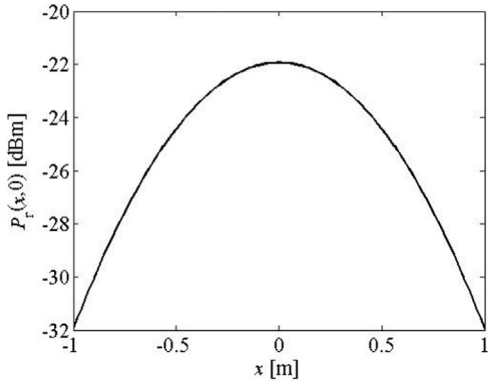

Fig. 8. Estimated required power along the x-axis for the 10 Gb/s system.

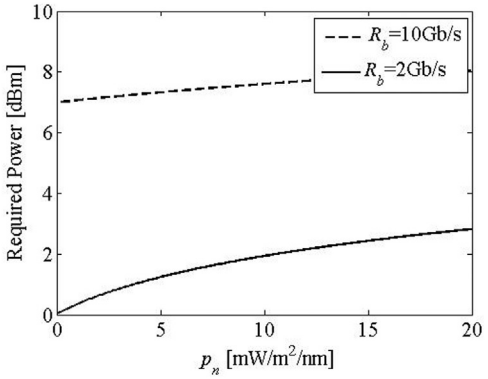

Fig. 9. Estimated required local oscillator and transmitter power to achieve an SNR-per-symbol equal to 20 dB at distance $\rho_0=1$ m from the transmitter projection on the receiver plane.

that even at 10 Gb/s, coherent detection does not impose significant power requirements.

4.4. Influence of ambient light noise

In our calculations up to now, we have neglected the ambient light noise ($P_{\text{amb}}=0$). We now discuss its influence in more detail. The ambient noise power P_{amb} is determined by [33]:

$$P_{\text{amb}} = p_n \Delta\lambda A_{\text{eff}}, \tag{28}$$

where p_n is the spectral irradiance of the ambient light, $\Delta\lambda$ is the optical bandwidth and A_{eff} is the effective receiver area perceived by the ambient light. The optical bandwidth can be limited by an optical filter $\Delta\lambda$. In Table 1, we have assumed that the optical filter bandwidth is 50 nm which is a typical value used in optical wireless implementations [33] in order not to limit the receiver field-of-view. The spectral irradiance can be measured or estimated using the model outlined in [34] and was implemented in [36]. Applying this model, we have estimated that the spectral irradiance at $\lambda=1550$ nm assuming that the room dimensions are 5 m × 5 m × 3.8 m and a single window covering most of the northern wall of the room. The window actually acts as a large secondary transmitter. We assume that the window irradiance is equal to the irradiance of sunlight, $p_{\text{sun}}\cong 0.2$ W/m^2/nm at $\lambda=1550$ nm [32]. We have also taken into account the irradiance produced by 16 halogen lamps placed in a rectangular grid at the ceiling with 1 m spacing. The irradiance of the lamps is taken $p_{\text{lamp}}=0.03$ W/m^2/nm. Using the formulas in [36] we calculated the average irradiance inside the room at various points at the receiver plane (x,y,0.8 m) placed on 2D grid with grid spacing $\Delta x=\Delta y=0.1$ m. The average light irradiance was approximately 9.6 mW/m^2/nm which we take as a typical irradiance p_n value in our calculations.

To combat the detrimental effect of ambient light-induced shot noise to the SNR, we can increase the local oscillator power P_{LO} and the transmitted power P_T. In fact, since the same laser can be used both for transmitting data and as an oscillator in Fig. 1(a) at a practical transceiver design, we set $P=P_T=P_{\text{LO}}$ and increase both powers by the same factor. Fig. 9 shows the required optical power P in order to obtain an SNR equal to 20 dB for various values of the ambient light irradiance, assuming that $A_{\text{eff}}=A_r$. The power calculations are based on (22) and (14) where we also included a thermal noise component $S_{\text{th}}=10^{-24}A^2$/Hz that however has negligible impact on the results. Fig. 9 suggests that the penalty induced by the ambient light noise is about 3 dB for the 2 Gb/s and 1 dB for the 10 Gb/s even for $p_n=20$ mW/m^2/nm.

In the calculations of Fig. 9, we have assumed that $A_{\text{eff}}=A_r$. However, the effective area A_{eff} for the ambient light noise largely depends on how the receiver is implemented. In an integrated receiver, light is usually focused on a waveguide at the device input. If the waveguide is monomode, then most of the incoherent background radiation will not couple well with the fundamental waveguide mode and will therefore not reach the photodiodes. This is also true, if the incoming light is first focused on a single mode fiber and then fed to the coherent receiver, in which case only a small portion of the background radiation will excite the fundamental mode. A more detailed analysis reveals that the effective area A_{eff} is related to the coherence length of the ambient light. Following the methodology outlined in [37,38] the incident ambient light field can be de described in terms of its correlation function $W_{\mu\nu}=<E_\mu(\mathbf{r}_1)E_\nu^*(\mathbf{r}_2)>$ by a Gauss–Schell model,

$$W_{\mu\nu}(\boldsymbol{\rho}_1,\boldsymbol{\rho}_2) = A_\mu A_\nu B_{\mu\nu} \exp\left(-\frac{\rho_1^2+\rho_2^2}{4\sigma^2} - \frac{|\boldsymbol{\rho}_1-\boldsymbol{\rho}_2|^2}{2\delta^2}\right), \tag{29}$$

where $\boldsymbol{\rho}_1$ and $\boldsymbol{\rho}_2$ are points on the receiving aperture, μ and ν refer to the x or the y component, σ determines the uniformity of the incident wave intensity while δ is related to the degree of spatial correlation. The amplitudes A_μ and $B_{\mu\nu}$ determine the average field intensity and the level of polarization correlation respectively. By back-propagating the guided mode of the waveguide one obtains an equivalent aperture mode at the receiving lens plane. This mode can be described by a Gaussian distribution of width $w_A=\lambda f_r/(\pi w_{\text{mode}})$ where w_{mode} is the width of the original waveguide mode discussed in Section 2.2. The hard receiving aperture can be replaced by a Gaussian aperture of width $W=2a(1/8)^{1/2}$ [39]. Retracing the calculation steps in [37,38], we find that if the average intensity is nearly constant over the aperture ($\sigma\to\infty$) and W is matched to w_A ($W=w_A$), then the coupling efficiency η into a single mode fiber is approximated by:

$$\eta \cong \frac{\frac{1}{4a^4}}{\left(\frac{1}{2a^2}+\frac{1}{2\delta^2}\right)^2 - \frac{1}{4\delta^4}}, \tag{30}$$

and if we assume that the spatial coherence length δ is much smaller than the aperture radius the efficiency is given by:

$$\eta \cong 4\delta^2/a^2 = \frac{4\pi\delta^2}{A_r}. \tag{31}$$

This result implies that the aperture area is actually $A_{\text{eff}}=4\pi\delta^2$ instead of $A_r=\pi a^2$ for partially coherent light. The coherence length of sunlight is of the order of tenths of wavelengths [40]. Taking $\delta=50\lambda$, Eq. (31) suggests that the ambient light coupling efficiency for the system at hand is $\eta\cong -43$ dB. Artificial light sources can have even more small coherence length [41] and hence even worst coupling efficiency. The above analysis which

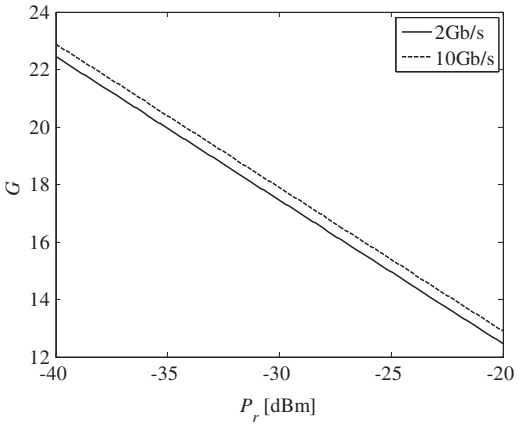

Fig. 10. Estimated coherent detection gain.

applies to diffuse multipath components as well, suggests that the effect of ambient light noise may be less detrimental than that illustrated in Fig. 9, because of the associated coupling inefficiencies.

5. Comparison with direct detection systems

It is useful to compare the performance of a coherent system with that of an equivalent direct-detection system occupying the same bandwidth and achieving the same data rate with the same bit error probability. The latter system relies on intensity modulation and we consider a single carrier 4-PAM which uses the same pulse shapes as the Q-PSK system and transmit 2 bits-per-symbol. Note that we neglect any multipath effects for the IM/DD system as well. In a practical IM/DD system, compensation schemes may have to be be incorporated for mitigating the frequency selective nature of the channel [36]. For the 4-PAM system, assuming that for that the maximum received power is P_d then the non-negative PAM symbols are given by $(m-1)RP_d/3 \;\; 1 \le m \le 4$ and the minimum symbol distance is therefore equal to $RP_d/3$. The symbol error rate is $P_4 = 3Q(\gamma_d)/2$ where $\gamma_d = RP_d/6/\sigma_d$ and σ_d is the variance of the additive noise, while the bit error probability is $P_b \cong 3Q(\gamma_d)/4$ [30]. For $P_b = 10^{-3}$, we find that $\gamma_d \cong 3$ and hence the required power is:

$$P_d^2 = \frac{36\gamma_d^2\sigma_d^2}{R^2} \cong \frac{72q\gamma_d^2 P_{\text{amb}}B}{R} \tag{32}$$

where we have assumed that the shot noise is dominant, i.e. $\sigma_d^2 \cong 2qR(P_{\text{amb}} + P_d)B \cong 2qRP_{\text{amb}}B$. Comparing (32) and (22) we obtain the following relation between the required received power in the case of IM/DD and coherent systems P_d and P_r respectively,

$$P_d \cong 3\frac{\gamma_d}{\gamma_c}\sqrt{\frac{P_{\text{amb}}P_{\text{LO}}P_r}{P_{\text{amb}} + P_{\text{LO}}}} \tag{33}$$

The above equation is applicable for shot-noise limited receivers. Assuming that $p_n \cong 10\ \text{mW/m}^2/\text{nm}$, $\Delta\lambda = 50$ nm and $A_R = 17.4\ \text{cm}^2$, we obtain $P_{\text{amb}} = 0.87$ mW. In addition as shown in Fig. 2, for an error rate of 10^{-3}, the required SNR value γ_c^2 is about 12 dB ($\gamma_c \cong 4$). Fig. 10 shows the coherent detection gain $G = P_d/P_r$ for the system at hand assuming two different LO powers corresponding to the 2 Gb/s and the 10 Gb/s design. We observe that the gain depends on the received power of the coherent system P_r and varies in the vicinity of 10 to 20 dB. For the 2 Gb/s system the gain can therefore be ≥ 20 dB especially near the edge of the coverage area where according to Fig. 6(a) is $P_r \cong -40$ dBm. For the 10 Gb/s where P_r is larger the gain is somewhat smaller. According to Fig. 7, at the edge of the coverage area the received power is equal to $\cong -32$ dBm the gain is approximately -18.5 dB. We should also note that while the transmission power for the coherent system quoted in Table 1 for the 2 Gb/s and 10 Gb/s are 1 mW and 5 mW which are less than 10 mW [35] and can be classified as Class-1 in terms of eye-safety, the IM/DD system requires more than 100 mW and 300 mW respectively to obtain the same error probability at the edge of the coverage area.

6. Conclusions

We have carried out a detailed design for coherent optical wireless systems intended for indoor applications. We have estimated the required signal-to-noise ratio at the receiver for a given linewidth-to-symbol duration product. We have also discussed in detail the transmitter and receiver optics and the trade-off between receiver area and transmitter power. We have shown that if the receiver plane is at a distance of 3 m from the transmitter then a circular coverage area of 1 m can be obtained by properly adjusting the transmitter optics while the power requirements that are well below those of commercially available narrow linewidth lasers, even at 10 Gb/s data rates. This can open a path towards establishing ultra-broadband wireless data networks in home/office settings or even in data centers and server farms. We have also analyzed the effect of ambient light noise and discussed the ambient light coupling efficiency reduction due to the partial coherent nature of the ambient light field. Finally we compared the performance of coherent detection and direct detection and shown a significant power gain in the former case of the order of 20 dB, near the edge of the coverage area.

Acknowledgments

The research reported in this paper was fully supported by the "ARISTEIA II" Action ("COWS" project) of the "Operational programme Education and Life Long Learning" and is co-funded by the European Social Fund (ESF) and the Greek State.

References

[1] P. Green, Fiber to the Home: The New Empowerment, Wiley-Interscience, New Jersey, 2005.
[2] C.F. Lam, The road to scalable 1 Gb/s FTTH access networks, in: Proceedings of the European Conference and Exhibition on Optical Communications (ECOC), vol. 1, no. 3, 2011, pp. 18–22.
[3] C.F. Lam, Passive Optical Networks: Principles and Practice, Academic Press, 2007.
[4] K. Grobe, J.-P. Elbers, PON in adolescence: from TDMA to WDM-PON, IEEE Commun. Mag. 46 (1) (2008) 26–34.
[5] T. Rokkas, T. Kamalakis, D. Katsianis, D. Varoutas, T. Sphicopoulos, Business prospects of wide-scale deployment of free space optical technology as a last-mile solution: a techno-economic evaluation, J. Opt. Netw. 6 (2007) 860–870.
[6] H. Elgala, R. Mesleh, H. Haas, Indoor optical wireless communication: potential and state-of-the-art, IEEE Commun. Mag. 49 (9) (2011) 56–62.
[7] D.C. O'Brien, G. Faulkner, Hoa Le Minh, O. Bouchet, M. El Tabach, M. Wolf, J.W. Walewski, S. Randel, S. Nerreter, M. Franke, K.-D. Langer, J. Grubor, T. Kamalakis, Home access networks using optical wireless transmission, in: Proceedings of the PIMRC 2008, IEEE 19th International Symposium on Personal, Indoor and Mobile Radio Communications, vol. 5, no. 1, 2008, pp. 15–18.
[8] A. Vahdat, M. Al-Fares, N. Farrington, R.N. Mysore, G. Porter, S. Radhakrishnan, Scale-out networking in the data center, IEEE Micro 30 (4) (2010) 29–415550998.
[9] X. Zhou, Z. Zhang, Y. Zhu, Y. Li, S. Kumar, A. Vahdat, B.Y. Zhao, H. Zheng, Mirror mirror on the ceiling: Flexible wireless links for data centers, Comput. Commun. Rev. 42 (4) (2012) 443–454.
[10] D. O'Brien, R. Turnbull, G. Hoa Le Minh, O. Faulkner, P. Bouchet, M. Porcon, E. El Tabach, M. Gueutier, L. Wolf, Grobe, L. Jianhui, High-speed optical wireless demonstrators: conclusions and future directions, J. Lightwave Technol. 30 (13) (2012) 2181–2187.

[11] M. Jafar-M, D.C. O'Brien, C.J. Stevens, D.J. Edwards, Evaluation of coverage area for a wide line-of-sight indoor optical free-space communication system employing coherent detection, IET Commun. 2 (2008) 18–26.
[12] G. Ntogari, T. Kamalakis, T. Sphicopoulos, Analysis of indoor multiple-input multiple-output coherent optical wireless systems, J. Lightwave Technol. 30 (3) (2012) 317–3246084693.
[13] K. Margariti, T. Kamalakis, Performance of coherent detection in optical wireless systems for high speed indoor communications, Opt. Quantum Electron. 0306–8919 (2014) 1–19.
[14] N. Farrington, G. Porter, S. Radhakrishnan, H.H. Bazzaz, V. Subramanya, Y. Fainman, G. Papen, A. Vahdat., Helios: a hybrid electrical/optical switch architecture for modular data centers, SIGCOMM Comput. Commun. Rev. 41 (4) (2010) 339–350.
[15] W. Shieh, X. Yi, Y. Ma, Q. Yang, Coherent optical OFDM: has its time come? J. Opt. Netw. 7 (2008) 234–255.
[16] E. Ip, A.P. Tao Lau, D.J.F. Barros, J.M. Kahn, Coherent detection in optical fiber systems, Opt. Express 16 (2008) 753–791.
[17] M. Nakazawa, K. Kikuchi, T. Miyazaki, High Spectral Density Optical Communication Technologies, 1st Edition, Springer-Verlag, Berlin Heidelberg, 2010.
[18] S.J. Savory, Digital coherent optical receivers: algorithms and subsystems, IEEE J. Sel. Top. Quantum Electron. 16 (5) (2010) 1164–1179.
[19] E. Siegman, Lasers, University Science Books, Mill Valley, CA, 1986.
[20] P.A. Bélanger, Beam propagation and the ABCD ray matrices, Opt. Lett. 16 (4) (1991) 196.
[21] J.W. Goodman, Introduction to Fourier Optics, Second Edition, McGraw-Hill, Inc., New York, NY, 1996.
[22] M. Abramowitz, I.A. Stegun, Handbook of Mathematical Functions with Formulas, Graphs, and Mathematical Tables, Dover Publications, New York, 1972.
[23] D. Marcuse, Loss analysis of single-mode fiber splices, Bell Syst. Tech. J. 56 (1977) 703.
[24] G. Einarsson, J. Strandberg, I.T. Monroy, Error probability evaluation of optical systems disturbed by phase noise and additive noise, IEEE J. Lightwave Technol. 13 (1995) 1847–1852.
[25] I. Fatadin, S.J. Savory, D. Ives, Compensation of quadrature imbalance in an optical QPSK coherent receiver, Photonics Technol. Lett., IEEE 20 (20) (2008) 1733–1735.
[26] T. Okoshi, Polarization control schemes for heterodyne and homodyne optical fiber communications, J. Lightwave Technol. LT-3 (6) (1985) 1232–1237.
[27] T.G. Hodgkinson, R.A. Harmon, D.W. Smith, Polarisation insensitive heterodyne detection using polarization scrambling, Electron. Lett. 23 (10) (1987) 513–514.
[28] B. Glance, Polarisation independent coherent optical receiver, J. Lightwave Technol. 5 (2) (1987) 274–276.
[29] D. Ly-Gagnon, S. Tsukamoto, K. Katoh, K. Kikuchi, Coherent detection of optical quadrature phase-shift keying signals with carrier phase estimation, J. Lightwave Technol. 24 (1) (2006) 12–21.
[30] J.G. Proakis, M. Salehi, Communication System Engineering, 2nd Edition, Prentice Hall, New Jersey, 2002.
[31] J.M. Kahn, J.R. Barry, Wireless infrared communications, Proc. IEEE 85 (2) (1997) 265–298.
[32] G. Dede, T. Kamalakis, D. Varoutas, Towards a roadmap for future home networking systems: an analytical hierarchy process approach, IEEE Syst. J. 5 (3) (2011) 374–384.
[33] G. Thuillier, M. Hersé, D. Labs, T. Foujols, W. Peetermans, D. Gillotay, P. C. Simon, H. Mandel, The solar spectral irradiance from 200 to 2400 nm as measured by the SOLSPEC spectrometer from the Atlas and Eureca missions, Solar Phys. 214 (1) (2003) 1–22.
[34] J.B. Carruthers, J.M. Kahn, Angle diversity for nondirected wireless infrared communication, IEEE Trans. on Commun. 48 (6) (2000) 960–969.
[35] A.M. Street, P.N. Stavrinou, D.C. O'Brien, D.J. Edwards, Indoor optical wireless systems – a review, Opt. Quantum Electron. 29 (3) (1997) 349–378.
[36] G. Ntogari, T. Kamalakis, T. Sphicopoulos, Performance analysis of decision feedback and linear equalization schemes for non-directed, indoor optical wireless systems, J. Commun. 4 (8) (2009) 565–571.
[37] M. Salem, G.P. Agrawal, Coupling of stochastic electromagnetic beams into optical fibers, Opt. Lett. 34 (2009) 2829–2831.
[38] M. Salem, G.P. Agrawal, Effects of coherence and polarization on the coupling of stochastic electromagnetic beams into optical fibers: errata, J. Opt. Soc. Am. A 28 (2011) 307.
[39] L.C. Andrews, R.L. Phillips, C.Y. Hopen, Laser Beam Scintillation with Applications, SPIE Press, 2001.
[40] S. Divitt, L. Novotny, Spatial coherence of sunlight and its implications for light management in photovoltaics, Optica 2 (2015) 95–103.
[41] C. Tsai, K. Tien, H. Lin, C. Lin, M. Chen, K. Chang, C. Wu, Analysis of coherence length of organic light emitting diodes, in: Frontiers in Optics/Laser Science XXIII/Organic Materials and Devices for Displays and Energy Conversion OSA Technical Digest (CD), Paper OWA6, 2007.